



Using tritium and ^{222}Rn to estimate groundwater discharge and thawing permafrost contributing to surface water in permafrost regions on Qinghai-Tibet Plateau

Chengwei Wan^{1,2,3,4} · Kai Li² · Sichen Shen⁵ · J. J. Gibson^{3,4} · Kaifang Ji^{1,2} · Peng Yi^{1,2} · Zhongbo Yu^{1,2}

Received: 21 May 2019

© Akadémiai Kiadó, Budapest, Hungary 2019

Abstract

On the Qinghai-Tibet Plateau, permafrost degradation and associated release of permafrost meltwater has undoubtedly modified the annual and seasonal streamflow patterns and influenced groundwater conditions. However, it is still unclear how extensively permafrost degradation has influenced surface and subsurface water systems due to very sparse observations. Isotope mass models combining tritium and ^{222}Rn measurements are developed here to quantify the contributions of groundwater discharge and thawing permafrost to rivers and lakes in the Source Area of the Yellow River. Results demonstrate the spatial variability of permafrost thaw impacts and confirm significant influence on surface and subsurface runoff processes including effects on water yield capacity and water drainage connectivity. While results to date are conclusive, further work to refine the method and extend observations is warranted.

Keywords Tritium · ^{222}Rn · Isotope mass balance model · Permafrost hydrology · Permafrost degradation · Source Area of the Yellow River

Introduction

Frozen ground including permafrost and seasonally frozen soil is a key component of the cryosphere which plays significant role in regulating energy exchange and water cycling on the Earth's surface, and is uniquely vulnerable to climate and environmental change [1–3]. Under the backdrop of global warming, high-latitude arctic and subarctic regions, as well as high elevation regions such as Qinghai-Tibet Plateau (QTP) with extensive permafrost, have undergone

remarkable permafrost degradation during the past several decades [1–6]. Substantial alteration of ground thermal regimes in these areas have also reshaped landscape features and resulted in alteration in regional hydrological and biogeochemical cycles [7]. Studies conducted in eastern Siberia, Canada's Northwest Territories and the Yukon River Basin have suggested positive correlations between streamflow discharge and permafrost degradation, and notably, have established that thawing permafrost not only contributes to streamflow in the warm season but also may influence or maintain base flow during the cold season [8–10]. Dramatic increases in discharge of the major rivers in Pan-Arctic watersheds have been observed in recent decades, largely attributed to thawing permafrost as well as increased hydrological connectivity between surface and subsurface flow systems [7, 11]. In some cases, enlargement of groundwater storage capacity due to permafrost degradation has counteracted increases in streamflow [12]. In other cases, deepening active layers have lowered groundwater levels, leading to delayed subsurface runoff, weaker precipitation-runoff responses, and a shift towards greater influence of groundwater discharge on streamflow [13]. In addition, degradation of permafrost is often associated with lake and wetland development, distribution and evolution, which is known

✉ Chengwei Wan
wanchengweidirk@hhu.edu.cn

¹ State Key Laboratory of Hydrology - Water Resources and Hydraulic Engineering, Nanjing 210098, China

² College of Hydrology and Water Resources, Hohai University, Nanjing 210098, China

³ Department of Geography, University of Victoria, P.O. Box 3060, STN CSC, Victoria, BC V8W 2Y2, Canada

⁴ InnoTech Alberta, 3-4476 Markham Street, Victoria, BC V8Z 7X8, Canada

⁵ College of Energy and Electrical Engineering, Hohai University, Nanjing 210098, China

to be influential in partitioning of surface and subsurface flows, often intensifying surface/subsurface interactions, and potentially leading to talik formation [6, 7]. While enhancement of hydraulic connectivity between surface water and subsurface flow systems under degrading permafrost conditions is widely noted and generally accepted, the impacts of permafrost degradation on streamflow remain a topic of debate [14].

Previous studies have demonstrated that continued permafrost degradation has modified streamflow patterns at seasonal and interannual timescales as permafrost meltwater augments water fluxes to rivers, thermokarst lakes and groundwater on the QTP [6, 13, 14]. In addition, changes and enhanced site-to-site variability in surface and subsurface water balances occur due to complex shifts in permafrost distribution at different stages of degradation, producing varying amounts of meltwater release from thawing permafrost [14]. Previous studies have qualified hydrological effects of warming permafrost, quantified contribution of supra-permafrost groundwater and melting ground ice to river discharge, and estimated proportions of thermokarst lake volumes using insitu observations, empirical or statistical simulations, and process-based models [5, 8, 10, 15, 16]. In general, observations were limited to individual landscape types, and were limited in duration and extent. As such, a knowledge gap still remains as to how permafrost degradation influences the contribution from thawing permafrost to surface and subsurface water systems at the regional scale on the QTP [17]. Complicated thermal processes related to permafrost would likely bring high uncertainty in numerical modelling, while traditional methods such as long-term monitoring and high frequency of hydrological surveys might be difficult or impractical to conduct in high-altitude cold regions [18–20]. In recent years, water isotope analysis has substantially been proven to be an effective way to obtain increased understanding of detailed permafrost hydrology. Isotope mass balance (IMB) using oxygen and hydrogen stable isotopes has been shown to be especially useful for estimating the contributions of various source waters to lakes and rivers, and has led to significant advances in hydrologic understanding [15–23]. Further understanding can be gained from naturally occurring radioactive isotope such as tritium (^3H) and radon (^{222}Rn) which can likewise be incorporated within IMB to produce quantitative results [18–20, 23–27]. The fate and transport of tritium in permafrost-related water mainly depends on ground temperature, so the increased tritium mobility as well as unique tritium signals in specific water bodies can provide additional insight into thawing permafrost processes as compared to stable isotopes alone, the latter often being influenced by evaporation that may mask original source water signatures [24, 26]. As ^{222}Rn from active subsurface inputs can be measured and used to assess the strength of subsurface connections to surface

water bodies, it is considered to be an ideal groundwater indicator [19, 20, 27].

The SAYR is characterized by a mosaic of different frozen ground types, including seasonally frozen soil, sporadic or isolated patches of permafrost, extensive discontinuous permafrost, and continuous permafrost, which is considered to represent temporal evolution of the permafrost thaw sequence [28]. Yi et al. [18] were the first to report the hydrological linkage between thawing permafrost and surface and subsurface water bodies in the SAYR via comparison of tritium signals. However, this paper did not examine spatial patterns or classify water bodies, nor did it quantify the hydrological effects of permafrost thawing. Preliminary observations by [19,20] found significant differences (1–2 order of magnitudes) in ^{222}Rn concentrations between groundwaters and surface waters, and these studies then applied IMB based on ^{222}Rn to estimate the groundwater fractions of 19% and 30%, respectively, in a small tributary with discontinuous permafrost, and a reach of the Yellow River near the outlet of the headwater region with seasonally frozen soil. Neither study was aimed at evaluating hydrological processes in different watershed types, nor did they examine seasonal differences or meltwater contributions to lakes or river discharge, largely due to limited sampling opportunities and logistical constraints.

Based on several field investigations carried out in SAYR, a more systematic and comprehensive water isotope dataset including tritium concentrations and ^{222}Rn activities has been established and will be reported in this paper. Additionally, the tritium contents in permafrost itself are measured, providing direct evidence that thawing permafrost is in fact feeding surface and subsurface water bodies. Previous studies [27, 28] have provided insightful discussions about using IMB model via ^{222}Rn to provide reliable estimates of groundwater discharge to rivers and lakes. Accordingly, the main purpose of this paper is to present, review and evaluate the theoretical basis for applying a combined IMB approach using ^{222}Rn and tritium as a method for evaluating seasonal groundwater and permafrost-thaw contributions to a range of surface water bodies, and ultimately to improve the understanding of the hydrological effects of permafrost degradation in the SAYR.

Study area

The Source Area of the Yellow River (SAYR) is situated in the northeastern part of Qinghai-Tibet Plateau between $95^{\circ}55'–98^{\circ}41'\text{E}$ and $33^{\circ}56'–35^{\circ}31'\text{N}$, and is the headwater catchment of the Yellow River, with a total area of $20,930\text{ km}^2$ (Fig. 1). Three mountain ranges form the watershed divide of the SAYR, including the Buqing Mountains in the north, Geshigeya Mountains in the west, and Bayan

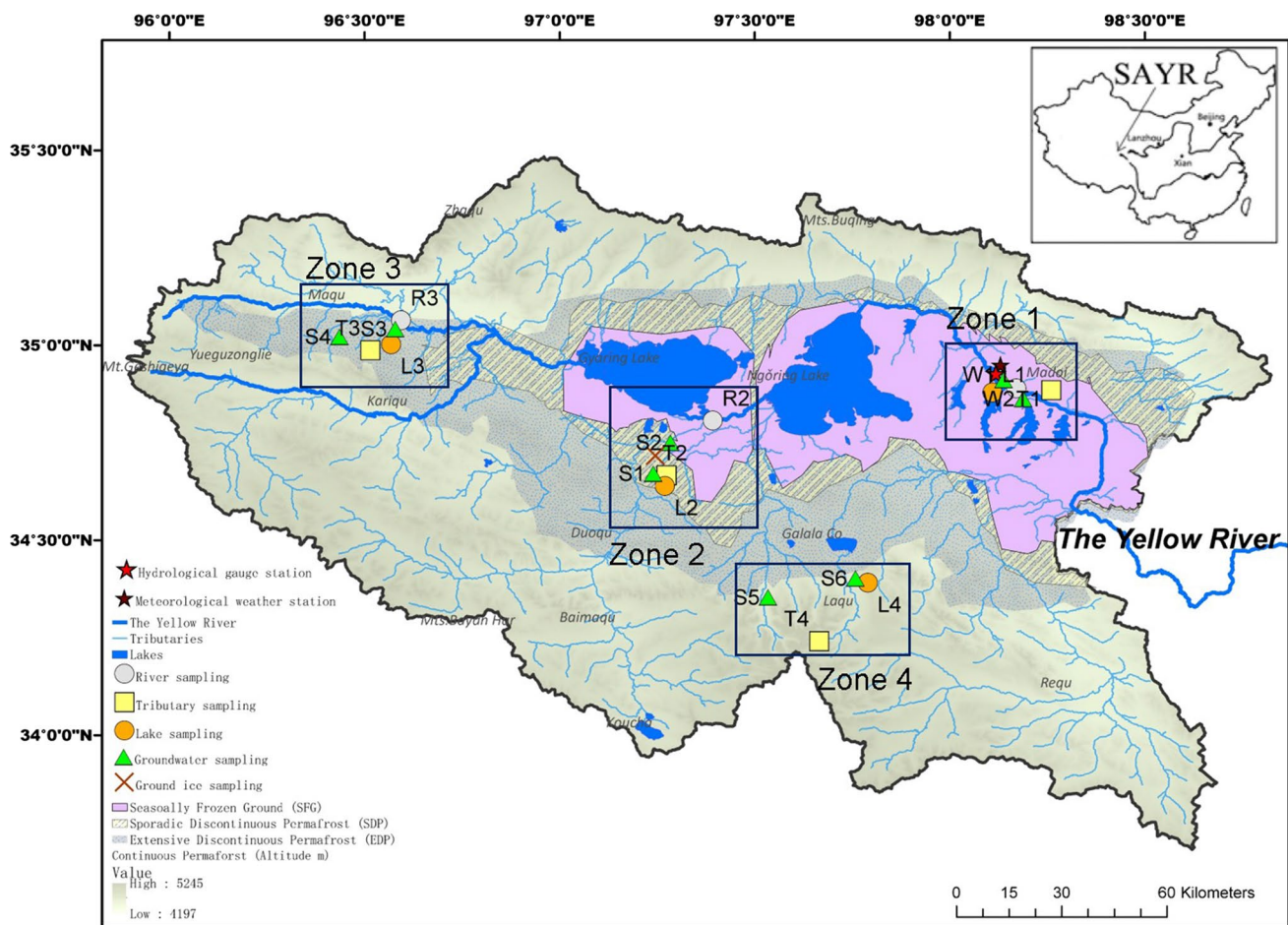


Fig. 1 The geographic location of the SAYR and sampling sites with permafrost distribution. The base map and permafrost distributions are referenced from [18, 33]

Har Mountains in the south. The Yellow River originates from the west, runs eastward and flows across the two big lakes (Gyaring and Ngoring lakes), and exits the headwater region in the east at Madoi after accumulating significant flow contributions from a number of tributaries and creeks draining the surrounding mountains. The elevation rises from 4200 m a.s.l in the eastern river valley to 5267 m a.s.l at the peak of Bayan Har [29]. This region is dominated by continental and semi-arid, alpine climate zones [30]. The mean annual air temperature (MAAT) is $-3.6\text{ }^{\circ}\text{C}$ for the 1956–2014, while the highest monthly average air temperature typically occurs in July ($7.8\text{ }^{\circ}\text{C}$) and the lowest in January ($-16.1\text{ }^{\circ}\text{C}$), as reported by the Meteorological Station in Madoi town. Average annual humidity is close to 50%. Aridity is also enhanced by low precipitation and high evaporation rates, given that annual total precipitation is near 320 mm while annual open water evaporation rates can exceed 1300 mm. Spring freshet conditions generally extend from March to May, whereas summer conditions are observed during June to August, autumn is observed from

September to November, and winter occurs from December to February.

Here, permafrost is classified as thermally unstable due to warm ground temperatures (mean annual ground temperature $> -2.0\text{ }^{\circ}\text{C}$), thin development (permafrost thickness $< 100\text{ m}$) and ice-rich features (high ice content near permafrost table), hence, permafrost is especially vulnerable to a warming climate [30, 31]. A complex mosaic of frozen ground types are currently observed across the region, including seasonally frozen soils, sporadic or isolated patches of permafrost, extensive discontinuous permafrost and continuous permafrost [28, 32]. Here, we chose four representative watersheds which span a typical gradient of frozen ground landscapes. Zone 1 is situated at the outlet of SAYR, which is mainly covered by seasonally frozen soil (coverage $> 90\%$). In general, soils in this zone are very dry, with silt, sand and gravels abundant along the lower river plains, and barren, sandy soils and notable desert expanses [31]. Zone 2 is located along the Noyring Lake shoreline area. This basin is a transitional zone characterized by

taliks along the lakeshore in seasonally frozen soils and sporadic discontinuous permafrost, which supports various landscapes ranging from sandy, alpine grassland to dense paludal meadow. The ground surface is mainly covered with silty sand and gravels. Zone 3 forms an extensive area in the western part of SAYR dominated by extensive discontinuous permafrost, with continuous permafrost also prevalent in high elevation areas. This area experiences enhanced permafrost degradation as revealed by features such as pingos and frozen palsas which have thawed and collapsed, forming thermokarst pits. Bogs are widespread, while sparse or sporadic permafrost (from residual thawing permafrost) are often associated with open-water wetlands [28]. Zone 4 occurs predominately above 4800 m.a.s.l. and is dominated by continuous permafrost. Here, permafrost appears to be relatively cold and stable, owing to low mean annual ground temperature (< -2 °C) and reduced active layer thickness (< 0.6 m), as well as greatest permafrost thickness (> 60 m) compared with other zones [31]. Peaty organic soils with thicknesses of up to 0.5 m above the permafrost table maintain high soil moisture content in the active layer, promoting favorable growing condition for dense and stable vegetation [18, 32].

Materials and methods

Field work and sampling sites

Field investigations were conducted in the four selected watersheds (Zone 1–Zone 4) during 16–24 April and 19–27 July 2014, 17–23 January 2015, and 20 May 2016. Daily

meteorological data (air temperature, precipitation, relative humidity and evaporation rates) were obtained from Madoi meteorological station (98.08°E, 34.57°N). Daily discharge data for the Yellow River were obtained from the hydrological gauge station, as shown in Fig. 2.

Three stream sites (R1–R3: from the Yellow River), 4 tributary sites (T1–T4), 4 lake sites (L1–L4) and 8 groundwater sites (wells, W1 and W2, and springs, S1–S6) were visited in the three seasons for water/liquid samples during 2014–2015 (Fig. 1). Note that precipitation and ground ice samples from 2016 were reported in a previous paper [33], although additional results are reported for the first time. Sampling locations were determined and recorded by handheld GPS (Garmin eTrex 30x) (detailed in Table 1). At each the stream site, upstream and downstream water (labeled as R_u and R_d) was sampled three times at reach intervals ranging from 1000 to 2000 m. As tributaries originated from small basins, upstream water was considered to be representative of the water sources and downstream water (up to 1600 m along tributary reaches) was considered to be representative of water exported from the basins. In total, 42 river samples (18 from the Yellow River and 24 from its tributaries), 12 lake samples, 24 groundwater samples (6 from wells and 18 from springs) and 5 ground ice samples were collected for isotopic analysis. 6 rain and snow event samples were also gathered opportunistically in Zone 1 and Zone 4 using a bucket.

Surface water samples were routinely collected at a depth of 30–40 cm below the water surface and as far away from the river banks and lakeshores as possible. For well water sampling, pumps were run for 15 min before sampling to remove any stagnant water in the well bores. For

Fig. 2 Variations of hydroclimatic parameters in SYAR from 20140101 to 20150531. The yellow bars indicate sampling times. (Color figure online)

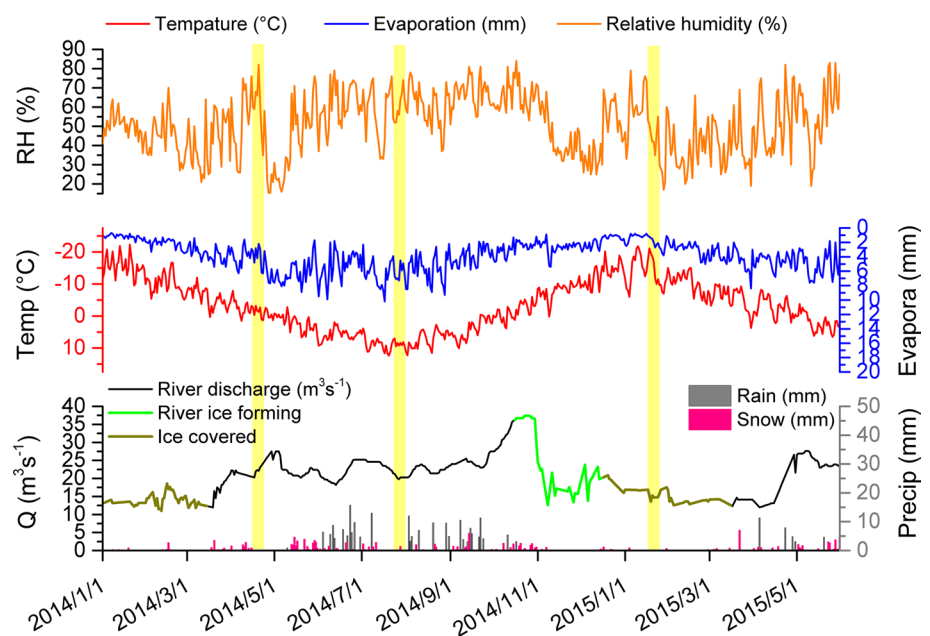


Table 1 Information of locations, sampling times, tritium and ^{222}Rn compositions

Sample ID	Type of water body	Latitude	Longitude	Sampling time	Tritium concentration			Radon activity	
					Bq/L	T.U	1 σ (T.U)	Bq/M ³	1 σ (Bq/M ³)
<i>Zone 1; Seasonally frozen ground</i>									
P1	Precipitation	34.8901	98.1706	2016/5/20	0.71 ^a	6.3 ^a	0.2 ^a		
				2016/5/20	0.71 ^a	6.3 ^a	0.2 ^a		
				2016/5/20	0.66 ^a	5.9 ^a	0.1 ^a		
R1_U	River	34.8901	98.1706	2014/4/16	1.69 ^b	11.2 ^b	0.2 ^b	780	163
				2014/7/22	1.91 ^b	10.5 ^b	0.1 ^b	1011	167
				2015/1/18	1.23	10.9	0.3	2509 ^c	345 ^c
R1_D	River	34.8901	98.1706	2014/4/16	1.63 ^b	11.4 ^b	0.2 ^b	1096	178
				2014/7/22	1.94 ^b	10.6 ^b	0.2 ^b	1765	234
				2015/1/18	1.68	11.7	0.2	5100 ^c	546 ^c
T1_U	Tributary	34.8851	98.2601	2014/4/16	1.35 ^b	12.0 ^b	0.3 ^b	896	124
				2014/7/22	1.26 ^b	11.2 ^b	0.1 ^b	1407	323
				2015/1/18	1.52	12.9	0.4	3471 ^c	578 ^c
T1_D	Tributary	34.8851	98.2601	2014/4/16	1.28 ^b	11.4 ^b	0.4 ^b	1074	154
				2014/7/22	1.18 ^b	10.5 ^b	0.2 ^b	1844	211
				2015/1/18	1.42	12.6	0.3	5899 ^c	544 ^c
L1	Lake	34.8794	98.1096	2014/4/16	1.28 ^a	12.1 ^a	0.2 ^a	386	83
				2014/7/22	1.10 ^a	12.0 ^a	0.1 ^a	499	54
				2015/1/18	1.28 ^a	11.4 ^a	0.3 ^a	865	121
W1	Groundwater	34.9111	98.1381	2014/4/16	1.64 ^b	13.9 ^b	0.3 ^b	7402	348
				2014/7/22	1.46 ^b	12.4 ^b	0.2 ^b	8961	1443
				2015/1/18	1.55	13.8	0.1	15,422 ^c	1043 ^c
W2	Groundwater	34.8622	98.1885	2014/4/16	1.64 ^b	13.6 ^b	0.1 ^b	7688	610
				2014/7/22	1.46 ^b	12.8 ^b	0.2 ^b	8469	1027
				2015/1/18	1.54	13.7	0.3	14,521 ^c	1025 ^c
<i>Zone 2; Sporadic discontinuous permafrost</i>									
R2_U	River	34.8075	97.3928	2014/4/19	1.63 ^b	14.5 ^b	0.2 ^b	2653	245
				2014/7/25	1.66 ^b	14.7 ^b	0.3 ^b	4120	153
				2015/1/20	1.76	15.6	0.2	9863 ^c	211 ^c
R2_D	River	34.8075	97.3928	2014/4/19	1.67 ^b	14.9 ^b	0.1 ^b	3506	332
				2014/7/25	1.64 ^b	14.6 ^b	0.3 ^b	5468	332
				2015/1/20	1.69	15.0	0.3	11,456 ^c	224 ^c
T2_U	Tributary	34.6669	97.2741	2014/4/17	1.69	14.3	0.2	2234	211
				2014/7/23	1.91	16.2	0.1	2988	324
				2015/1/19	1.81	16.1	0.1	4200 ^c	223 ^c
T2_D	Tributary	34.6669	97.2741	2014/4/17	1.63	13.8	0.3	3145	456
				2014/7/23	1.94	16.5	0.3	3917	234
				2015/1/19	1.68	14.3	0.4	7894 ^c	412 ^c
L2	Lake	34.6395	97.2700	2014/4/17	1.85 ^a	16.4 ^a	0.5 ^a	1233	223
				2014/7/23	1.71 ^a	15.2 ^a	0.1 ^a	2311	246
				2015/1/19	1.87 ^a	16.6 ^a	0.2 ^a	6522 ^c	566 ^c
G1	Ground ice (0.5 m)	34.7177	97.2458	2016/5/20	2.16 ^a	19.2 ^a	0.1 ^a		
G2	Ground ice (0.8 m)			2016/5/20	2.21 ^a	19.6 ^a	0.1 ^a		
G3	Ground ice (1.2 m)			2016/5/20	2.34 ^a	20.8 ^a	0.0 ^a		
G4	Ground ice (2.0 m)			2016/5/20	2.47 ^a	21.9 ^a	0.1 ^a		
G5	Ground ice (3.0 m)			2016/5/20	2.75 ^a	24.4 ^a	0.2 ^a		
S1	Supra-permafrost groundwater	34.6707	97.2405	2014/4/17	1.90	11.9	0.1	8650	988
				2014/7/23	1.92	13.1	0.2	9784	764

Table 1 (continued)

Sample ID	Type of water body	Latitude	Longitude	Sampling time	Tritium concentration			Radon activity	
					Bq/L	T.U	1 σ (T.U)	Bq/M ³	1 σ (Bq/M ³)
S2	Supra-permafrost groundwater	34.7498	97.2845	2015/1/19	1.26	11.2	0.1	18,655 ^c	1122 ^c
				2014/4/17	1.90	10.8	0.1	8966	536
				2014/7/23	1.54	13.7	0.2	9421	780
				2015/1/19	1.29	11.5	0.4	19,874 ^c	1314 ^c
<i>Zone 3; Plateau discontinuous permafrost</i>									
R3_U	River	35.0645	96.5941	2014/4/19	1.86	16.5	0.2	4560	174
				2014/7/25	1.89	16.8	0.2	6745	563
				2015/1/20	1.90	16.9	0.2	10,556 ^c	1045 ^c
R3_D	River	35.0645	96.5941	2014/4/19	1.87	16.6	0.2	5620	319
				2014/7/25	1.90	16.9	0.3	10,210	426
				2015/1/20	1.93	17.1	0.3	13,623 ^c	1444 ^c
T3_U	Tributary	34.9874	96.5149	2014/4/19	1.67	14.8	0.1	6788	345
				2014/7/25	1.80	16.0	0.2	6863	689
				2015/1/20	1.81	16.1	0.3	7865 ^c	855 ^c
T3_D	Tributary	34.9874	96.5149	2014/4/19	1.71	15.2	0.3	7956	190
				2014/7/25	1.79	15.9	0.2	9536	422
				2015/1/20	1.80	16.0	0.1	8755 ^c	675 ^c
L3	Lake	35.0031	96.5684	2014/4/19	2.31	20.6	0.1	3786	22
				2014/7/25	2.33	20.7	0.3	5423	766
				2015/1/20	2.30	20.4	0.3	9862 ^c	880 ^c
S3	Supra-permafrost groundwater	35.0417	96.5791	2014/4/19	1.91	17.0	0.2	12,004	897
				2014/7/25	2.03	18.0	0.2	15,336	902
				2015/1/20	1.71	15.2	0.2	21,057 ^c	1890 ^c
S4	Supra-permafrost groundwater	35.0217	96.4363	2014/4/19	1.89	16.8	0.1	14,071	1301
				2014/7/25	2.24	19.9	0.1	24,100	1110
				2015/1/20	1.61	14.3	0.0	24,512 ^c	2798 ^c
<i>Zone 4; Continuous permafrost</i>									
P2	Precipitation	34.2415	97.6653	2016/5/20	0.98 ^a	8.7 ^a	0.3 ^a		
				2016/5/20	0.90 ^a	8.0 ^a	0.1 ^a		
				2016/5/20	0.91 ^a	8.1 ^a	0.2 ^a		
T4_U	Tributary	34.2415	97.6653	2014/4/21	2.07	18.4	0.1	13,201	2167
				2014/7/26	2.08	18.5	0.2	7563	544
				2015/1/22	2.15	19.1	0.3	12,032	1223
T4_D	Tributary	34.2415	97.6653	2014/4/21	2.02	17.9	0.3	14,863	2343
				2014/7/26	2.09	18.6	0.2	10,235	790
				2015/1/22	2.14	19.0	0.2	13,561	855
L4	Lake	34.3912	97.7900	2014/4/21	1.98	17.6	0.2	6533	1121
				2014/7/26	2.02	17.9	0.2	7563	2118
				2015/1/22	2.30	17.3	0.1	14,124	1330
S5	Supra-permafrost groundwater	34.3534	97.5345	2014/4/21	1.46	13.0	0.2	34,568	3212
				2014/7/26	1.64	14.5	0.3	31,562	2245
				2015/1/22	1.27	11.3	0.3	41,230	4229
S6	Supra-permafrost groundwater	34.4019	97.7586	2014/4/21	1.48	13.2	0.2	28,966	1500
				2014/7/26	1.66	14.7	0.2	34,569	6197
				2015/1/22	1.36	12.1	0.1	37,456	2281

^aPublished data from [33]^bPublished data from [18]^cPublished data from [20]

the ground ice samples, 5 deep-buried ground ice samples were obtained from an 3-m depth ice core obtained by drilling into the ground surface to various depths as recorded in Table 1. In total, 56 of 89 points for tritium concentrations and 36 of 58 points for ^{222}Rn activities are newly reported data published here for the first time.

Liquid water samples were stored in 250 ml glass bottles (WAT-250 system; DurrIDGE Co) for ^{222}Rn measurement and 500 ml high-density polyethylene bottles for tritium analysis, respectively, ensuring minimal headspace and tightly sealed lids to minimize both degassing of ^{222}Rn and moisture exchange with the atmosphere [20]. Ice samples were preserved and kept frozen during transport, and then melted in the lab for the first time at room temperature in sealed bottles before analysis. Other liquid samples were refrigerated at 4 °C until analysis.

Isotopic analysis

^{222}Rn activity in the liquid samples was analyzed by an automatic radon monitor RAD7 and the RAD H₂O accessory (DurrIDGE Company, USA) within 3–6 h after collection from the water bodies. Four count cycles of 20 min were used for each sample with a 20 min count time for each cycle. ^{222}Rn activities are reported in Bq/m³ with analytical uncertainty varying by sample as determined by standard measurement errors.

For the tritium analysis, samples were returned to the State Key Laboratory of Hydro–Water Resources and Hydraulic Engineering, Nanjing, China. Tritium concentration measurements were completed using a liquid scintillation counting spectrometer (Tri–Carb 3170 TR/SL). Tritium concentrations results are reported in tritium units (T.U) with total analytical uncertainty of less than 0.6 TU for all samples. Tritium values were normalized by the correction of radioactive decay to 20 May 2016 to enable intercomparison of samples collected on different dates. It should be noted that ^{222}Rn activity data for 2015 were previously published [20], as were Zone 1 and Zone 2 tritium data [18, 33], although the present comparison is more comprehensive and provides significant new hydrological insight.

Development of IMB models

Along a specified river reach, groundwater–surface water interactions can be quantified based on ^{222}R isotope mass balance provided there are significant differences in ^{222}Rn activities between surface and subsurface water sources [27]. According to the mass conservation theory and considering the variation of ^{222}Rn activities in the natural environment, the basic water mass balance and isotope mass balance equation (river model) can be expressed as follows along a river reach [19, 20, 27]:

$$Q_d = Q_u + Q_g \quad (1)$$

$$Q_d C_d = Q_u C_u e^{-\alpha_1 L} + \int_0^L Q_g C_g e^{-\alpha_1 x} / L dx \quad (2)$$

where Q_u , Q_d and Q_g are upstream, downstream discharges and total recharges of groundwater to the river reach (m³/s), respectively; C_u , C_d and C_g are the ^{222}Rn activities in upstream water, downstream water and groundwater (Bq/m³), respectively; L is the distance between upstream and downstream sampling sites (m); and α is the total loss coefficient (m⁻¹).

Equations (1) and (2) should only be applied under strict application conditions, assumptions for which have been summarized previously [20, 27, 34]. The main assumptions include: 1. Precipitation and evaporative effects are negligible, 2. River cross-sections are well mixed vertically, so that sampled water at one site are representative of the entire depth profile of a river cross-section, 3. Groundwater recharge is the only source of ^{222}Rn in river water, and that groundwater recharge is uniformly distributed along the river bank along the reach, and 4. Gas exchange and radioactive decay are the only sinks for ^{222}Rn , while the contribution of ^{222}Rn from decay of ^{226}Ra in sediments and hyporheic exchange are considered negligible [35–37].

Radioactive decay and degassing consist of the total loss coefficient (α_1) [35]:

$$\alpha_1 = \beta + \gamma \quad (3)$$

$$\beta = \frac{\lambda_{\text{Rn}}}{v} \quad (4)$$

$$\gamma = \frac{D^{0.5}}{v^{0.5} h^{1.5}} \quad (5)$$

$$-\log D = \frac{980}{T_{\text{air}}} + 1.59 \quad (6)$$

where β and γ are the decay coefficient (m⁻¹) and degassing coefficient (m⁻¹), respectively; $\lambda_{\text{Rn}} = 2.08 \times 10^{-6} \text{ s}^{-1}$ is the radioactive decay coefficient; v is the average velocity of the river discharge (m/s¹); D is the molecular diffusion coefficient of gas (m²/s¹); h is the average river water depth (m); and T_{air} is the air temperature (K).

Similarly, we improved the ^{222}Rn box model based on water and isotope mass balance theory for lakes [38, 39] to account for the sources of radon from sediment diffusion and the decay of dissolved ^{226}Ra :

$$\frac{V_g (C_g - C_s)}{V_L} - \frac{F_{\text{degas}} A}{V_L} - \lambda_{\text{Rn}} C_s = 0 \quad (7)$$

where V_g is the groundwater recharge volume (m^3), V_L is the total lake volume (m^3); C_g and C_s are the ^{222}Rn activities in groundwater and lake water respectively; F_{degas} is the flux density of ^{222}Rn degassing to the atmosphere ($\text{Bq}/m^2 \text{ d}$) and A is the lake surface area (m^2) [40].

$$F_{\text{degas}} = k(C_s - \alpha_2 C_a) \quad (8)$$

$$k = 0.45 u_{10}^{1.6} \left(\frac{S_c}{600} \right)^{-b} \quad (9)$$

$$S_c = \nu/D \quad (10)$$

$$u_{10} = u \left[0.097 \ln \left(\frac{h}{10} \right) + 1 \right]^{-1} \quad (11)$$

$$\alpha_2 = 0.105 + 0.405 e^{-0.05027(T_{\text{air}} - 273.15)} \quad (12)$$

where k is the gas transfer coefficient (m/s), α_2 is the Ostwald's solubility coefficient, C_a is the ^{222}Rn activities in atmosphere; u_{10} is the wind velocity at 10 m height above the water surface (m/s), which can be estimated via the measured wind velocity (u) at height (h) in Eq. (11) [41]; S_c is the Schmidt number determined by the kinematic viscosity (ν) and molecular diffusion coefficient of gas (D); $b=0.5$ when $u_{10} > 3.6 \text{ m/s}$ and $b=0.667$ when $u_{10} < 3.6 \text{ m/s}$.

The accurate measurement of real-time river flow and lake water volume in this high-elevation and remote area are sparse for both main stream channels of greater than 10 m width as well as shallow tributaries [20] such that conventional reach mass balance assessment is difficult. Consequently, it is easier to measure the ^{222}Rn activities in upstream water, downstream water and groundwater as well as the climatic and physical parameters essential to application a radon balance. This permits estimation of the ratios of Q_g/Q_d and V_g/V_L which represent the relative contribution of groundwater recharge to river discharge and lake water volumes, respectively.

It is noted as an important consideration that groundwater in Zone 2 to Zone 4 was considered to have two components; one being supra-permafrost water originating from precipitation, and the other being thawing permafrost (ground ice). As such, the fraction ratio of melt ground ice to groundwater (X_{gi}) can be estimated by mass balance with several assumptions, as follows [6, 17, 42, 43]: 1. There are significant differences in concentrations of chemical or isotopic tracers in the two initial water components, which are the precipitation-related supra-permafrost water and ground ice individual to recharge to the groundwater. 2. The observed temporal variations of concentration of tracer in groundwater are naturally reflected the temporal fluctuating proportion of water

components. Thus, the contributing fraction of ground ice can be expressed as:

$$X_{\text{gi}} = \frac{T_{\text{gw}} - T_p}{T_{\text{gi}} - T_p} \quad (13)$$

where T_{gw} , T_p and T_{gi} are the concentrations of tracer in groundwater, precipitation and ground ice, respectively. Then multiplying Q_g/Q_d by X_{gi} as well as multiplying V_g/V_L by X_{gi} yields the contributing fractions of thawing ground ice to river discharge and to lake volume, respectively.

In this study, air temperature (T_{air}) and wind velocity (u) were measured using a Multifunctional Environmental Meter (RH87, OMEGA), and river flow velocity (ν) was measured using a portable current meter (81M/FP-211) with a measuring accuracy of $\pm 0.1 \text{ m/s}$. River depth was measured manually using a measuring staff. Ratio of A/V_L for individual lakes was based on previously reported data on ecological environmental geology in SAYR (2001–2004) [18, 28]. All parameters used in the models are shown in Tables 2, 3 and 4.

Results

Tritium concentrations in water bodies

Notably, precipitation samples show the depleted tritium concentrations and narrowly range between 5.9 and 8.7 T.U, values slightly reduced compared to present-day precipitation (10–20 T.U) as observed in interior North America at similar latitudes, e.g. the Sierra Nevada, and Ottawa, Canada (Fig. 3a) [44]. While ground ice samples share the highest tritium concentrations, ranging between 19.2 and 24.4 T.U, there is a remarkable increasing trend in the tritium concentrations from top (near earth surface) to bottom in the ground ice profile, which implies that younger ground ice (shallower buried) formed from a higher proportion of modern (post-1950s) precipitation, as reported by [33]. Statistically significant differences in tritium concentrations between precipitation and ground ice allows an estimate of the fraction of melted ground ice in groundwater to be separated from the fraction of precipitation by Eq. (13).

The greatest fluctuations of tritium values are noted for both lake water and groundwater, which range from 11.4 to 20.7 T.U and 10.8 to 19.9 T.U, respectively. A significantly statistical difference is found between lake water, with mean value of 16.5 T.U, and groundwater, with a mean value of 13.8 T.U based on t test ($p=0.023$). In contrast, lake water is undistinguishable from ground ice ($p < 0.005$). There are also no significant differences measured among stream water, tributary water and groundwater.

Table 2 Summary of parameters used in the river model in Eqs. (1)–(6)

Sampling sites	Sampling date	C_u (Bq/m ³)	C_d (Bq/m ³)	C_g (Bq/m ³)	Air temp (°)	River velocity (m/s)	h (m)	L (m)
R1	2014/4/16	780	1096	7545	-2.7	1.2	1.80	2000
	2014/7/22	1011	1765	8715	8.7	2.9	2.10	2000
	2015/1/18	2509	5100	14,972	-21.1	0.8	1.50	2000
T1	2014/4/16	896	1074	7545	-2.7	1.4	0.60	1000
	2014/7/22	1407	1844	8715	8.7	3.1	0.90	1000
	2015/1/18	3471	5899	14,972	-21.1	0.4	0.30	1000
R2	2014/4/17	2653	3506	8808	-3.0	2.6	1.35	980
	2014/7/23	4120	5468	9603	7.4	2.5	1.69	980
	2015/1/19	9863	11,456	19,265	-19.6	1.6	1.32	980
T2	2014/4/17	2234	3145	8808	-3.0	2.6	0.90	850
	2014/7/23	2988	3917	9603	7.4	2.3	1.30	850
	2015/1/19	4200	7894	19,265	-19.6	1.2	0.50	850
R3	2014/4/19	4560	5620	13,038	-3.2	4.1	1.10	1300
	2014/7/25	6745	10,210	19,718	9.5	2.4	1.40	1300
	2015/1/20	10,556	13,623	22,785	-18.6	1.0	1.00	1300
T3	2014/4/19	6788	7956	13,038	-3.2	2.3	0.50	1600
	2014/7/25	6863	9536	19,718	9.5	2.6	0.65	1600
	2015/1/20	7865	8755	22,785	-18.6	0.5	0.30	1600
T4	2014/4/21	13,201	14,863	31,767	-2.7	1.6	0.36	1450
	2014/7/26	7563	10,235	33,066	8.4	1.8	0.56	1450
	2015/1/22	12,032	13,561	39,343	-11.7	1.1	0.31	1450

Table 3 Summary of parameters used in the lake model in Eqs. (7)–(12)

Sampling sites	Sampling date	C_s (Bq/m ³)	C_g (Bq/m ³)	Air temp (°)	V/A	Wind velocity (m/s)
L1	2014/4/16	386	15,000	-2.7	1.6	1.2
	2014/7/22	499	8715	8.7	1.6	1.2
	2015/1/18	865	14,971.5	-21.1	1.6	1.2
L2	2014/4/17	1233	8808	-3	1.6	4
	2014/7/23	2311	9602.5	7.4	1.6	2.3
	2015/1/19	6522	19,264.5	-19.6	1.6	1.2
L3	2014/4/19	3786	13,037.5	-3.2	1.6	2.8
	2014/7/25	5423	19,718	9.5	1.6	2.4
	2015/1/20	9862	22,784.5	-18.6	1.6	2.3
L4	2014/4/21	6533	31,767	-2.7	1.6	2.9
	2014/7/26	7563	33,065.5	8.4	1.6	2.6
	2015/1/22	14,124	39,343	-11.7	1.6	3

Tritium concentrations in stream water and tributary water both span wide ranges of 10.5–17.5 T.U and 10.5–16.5 T.U, respectively, with average values of 14.2 and 14.5 T.U, respectively, which are lower than lakes. It can be inferred that permafrost meltwater is likely to be more interactive with thermokarst lakes than surface runoff and groundwater systems.

Overall ²²²Rn activities

The results of dissolved ²²²Rn in Fig. 3b show distinct contrast in activity levels between surface water (stream, tributary and lake) and groundwater. The average ²²²Rn activity measured in stream water is 5591 Bq/m³, with an observed range from 780 to 13,623 Bq/m³, and is similar to tributary water which averages 6591 Bq/m³, ranging from 896

Table 4 Summary of parameters used in the separation of groundwater components in Eq. (13)

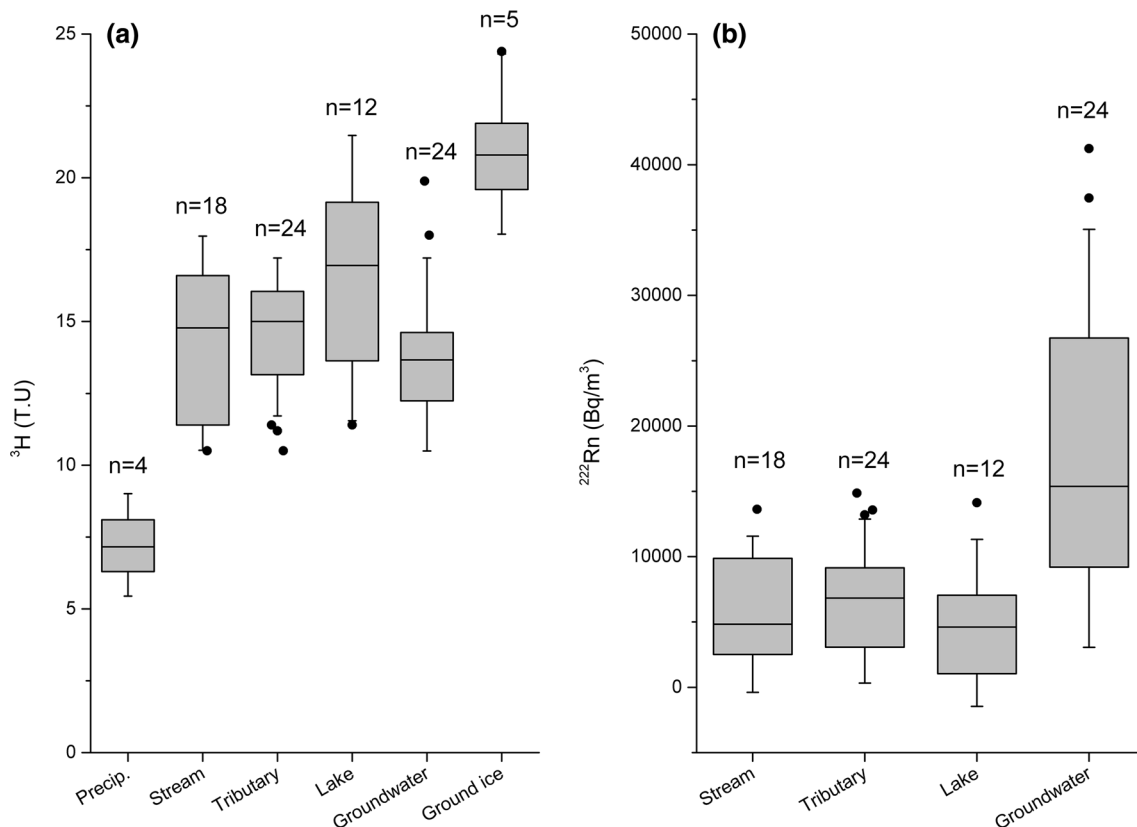
Sampling sites	Sampling date	T_{gw} (T.U)	T_{gi} (T.U)	T_{p} (T.U)
Zone 2	2014/4/17	11.4	21.2	6.2
	2014/7/23	13.4	21.2	6.2
	2015/1/19	11.4	21.2	6.2
Zone 3	2014/4/19	16.9	21.2	6.2
	2014/7/25	18.9	21.2	6.2
	2015/1/20	14.7	21.2	6.2
Zone 4	2014/4/21	13.1	21.2	8.3
	2014/7/26	14.6	21.2	8.3
	2015/1/22	11.7	21.2	8.3

to 14,893 Bq/m³. Lake water is found to have lower ²²²Rn activities, varying from 386 to 14,124 Bq/m³ and averaging 4926 Bq/m³. ²²²Rn activities in groundwater span a wide range from 7402 to 41,230 Bq/m³ with an average value of 19,052 Bq/m³, which differs significantly from surface waters. It is noticeable that the ²²²Rn activities in stream and tributary water sampled on the downstream reaches are higher than upstream reaches for each site in all seasons, which confirms that groundwater recharges to rivers all

year. The slightly higher ²²²Rn activities in tributary water as compared to rivers may reflect a quick or more direct linkage between small creeks and groundwater. Groundwater recharge to streams and lakes may be associated with longer residence times and deeper flowpaths, and in some cases may be diluted by more efficient hyporheic zone flushing, thus reducing ²²²Rn activities slightly. Note that ²²²Rn is not detectable in ground ice meltwater, thus, permafrost meltwater contributions to groundwater may only be evaluated by considering measurable differences in tritium concentrations in water sources which comprise the groundwater.

Spatial and temporal distributions of tritium and ²²²Rn

Figure 4a, b illustrates the spatial and temporal characteristics of tritium and ²²²Rn activities in various water bodies. Tritium concentrations in stream water decrease substantially from upstream to downstream (R3 to R1), which are shown to be reduced from 16.8 ± 0.2 T.U to 11.1 ± 0.5 T.U, respectively. Tritium concentrations in tributary water show a progressive increase depending on permafrost zones, where the average tritium content is 11.8 ± 0.9 T.U for tributary locations draining seasonally frozen ground (Zone 1),

**Fig. 3** Box plots showing values of tritium (a) and ²²²Rn (b) in water bodies. The whisker is defined by 1.5 times of standard deviation (SD)

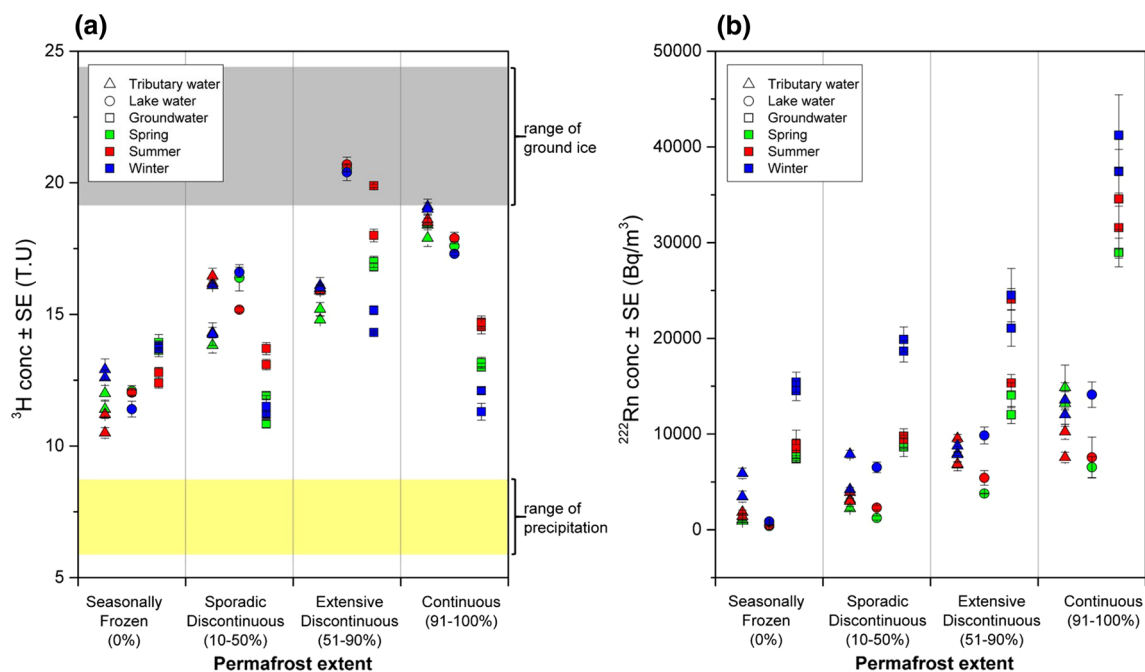


Fig. 4 **a** ^3H concentrations, and **b** ^{222}Rn activities in water bodies located in zones with different permafrost extents. Each sample is shown as a separate data point. Triangles represent tributary water samples, circles represent lake water samples, squares represent groundwater samples, while green color represents samples in spring

values of 15.2 ± 1.2 T.U. are found for sporadic discontinuous permafrost tributaries (Zone 2), values of 15.7 ± 0.5 T.U. are found for extensive discontinuous permafrost tributaries, and values of 18.6 ± 0.4 T.U. are found for continuous permafrost tributaries (Zone 4). The highest tritium concentrations are measured in lake water (20.6 ± 2.0 T.U.) and groundwater within extensive discontinuous permafrost (16.9 ± 2.0 T.U.). Tritium values of lake water are higher than river water and groundwater in discontinuous permafrost regions (Zone 2 and Zone 3). In continuous permafrost areas (Zone 4), there is a specific order noted for tritium enrichment, as follows: rivers (18.6 ± 0.4 T.U.) > lake (17.6 ± 0.3 T.U.) > groundwater (13.1 ± 1.3 T.U.). However, this order is reversed in permafrost free areas (Zone 1). Apparently, tritium concentrations are correlated with permafrost extent, and may be a useful index of meltwater contributions to water bodies.

Consistent with the tritium signals, spatial patterns of ^{222}Rn are also informative and systematic. ^{222}Rn activity in each water body appears to increase as regional permafrost coverage increases. The greatest differences in ^{222}Rn activity between groundwater and surface water occur in the continuous permafrost region (Zone 4), where the average value of ^{222}Rn activities in groundwater is commonly at least $20,000$ Bq/m 3 greater than the surface water. Moreover, there are no statistical differences in ^{222}Rn activity between river water and lake water in permafrost regions (Zone 2–4),

season, red color represents samples in summer season and blue color represents samples in winter season. Error bars are analytical uncertainty (1σ) of samples, also termed as standard error (SE). (Color figure online)

but river water (2238 ± 169 Bq/m 3) is distinctly higher than lake water (583 ± 250 Bq/m 3) in areas without permafrost (Zone 1).

Groundwater displays the greatest fluctuation in tritium contents due to seasonality. Higher tritium concentrations in groundwater often occur in summer in permafrost-affected areas (Zone 2–4), but in spring and winter in non-permafrost areas (Zone 1). The seasonal variation of tritium in other water bodies is more complicated. Winter is characterized by highest ^{222}Rn activities both in lake water and groundwater in all zones. Peak ^{222}Rn activities in rivers appears to reflect lag in timing of groundwater contributions across different permafrost zones, whereby it appears earliest during spring freshet within continuous permafrost, but is delayed to mid-summer in extensive discontinuous permafrost, and until late winter in seasonally frozen ground and sporadic discontinuous permafrost zones.

Estimation of groundwater and ground ice melt contributing to rivers and lakes

The proportions of groundwater and ground ice contributing to streamflow (shown in Fig. 5a), tributary flow and lake water volume (shown in Fig. 6a, b) are estimated from ^{222}Rn activities and tritium concentrations for three seasons at each surface water site using Eqs. (1)–(13). The proportion of

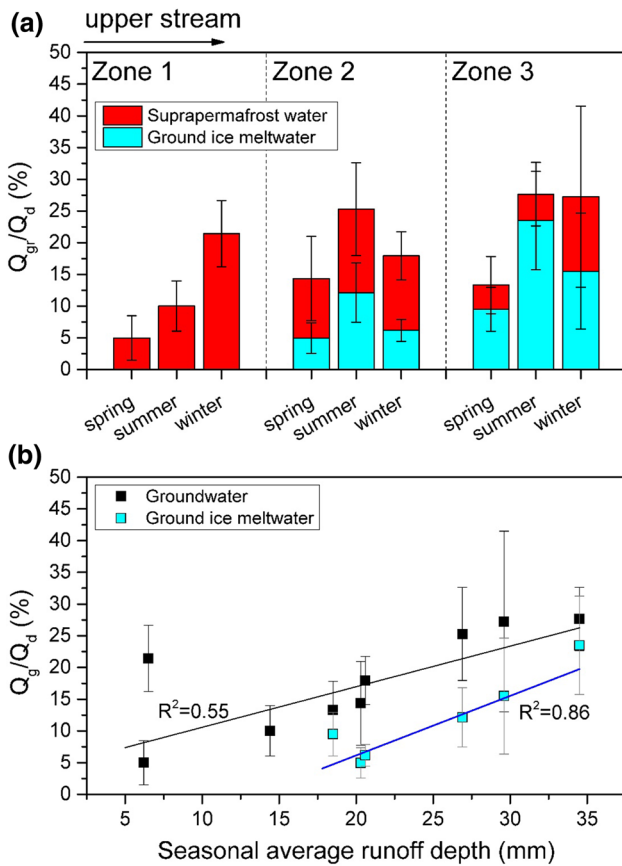


Fig. 5 **a** Estimated contribution ratios of groundwater and ground ice to streamflow in Zone 1–Zone 3 in the three seasons, and **b** relationship between groundwater and ground ice ratios and mean seasonal average runoff depths of 1995–2005. Error bars represent \pm standard error

groundwater discharge to streamflow is $5 \pm 4\%$ in the spring season and gradually increases to $10 \pm 4\%$ in summer, and reaches a maximum of $21 \pm 5\%$ in the winter season in Zone 1. In Zone 2 and Zone 3, the greatest proportion of groundwater contribution to streamflow is noted to be up to $25 \pm 7\%$ and $28 \pm 5\%$, respectively, which occurs in the summer season. In winter, the proportion of groundwater reduces somewhat to $18 \pm 4\%$ in Zone 2, while in Zone 3 it is little different than in summer, with a relatively high ratio of $27 \pm 14\%$. In the three seasons, the proportion of melting ground ice to streamflow in Zone 3 is nearly twice that of Zone 2, as the groundwater in Zone 3 stores significantly more meltwater from ground ice, which accounts for 57–85% of the total volume compared with that in Zone 2, where groundwater appears to be less than 50% from melted ground ice sources.

The proportion of groundwater discharge contributing to tributary flow appears to soar from $3 \pm 3\%$ in spring to $29 \pm 6\%$ in winter in seasonally frozen ground and from $14 \pm 8\%$ in spring and $26 \pm 4\%$ in winter in sporadic discontinuous permafrost. By contrast, a small decrease

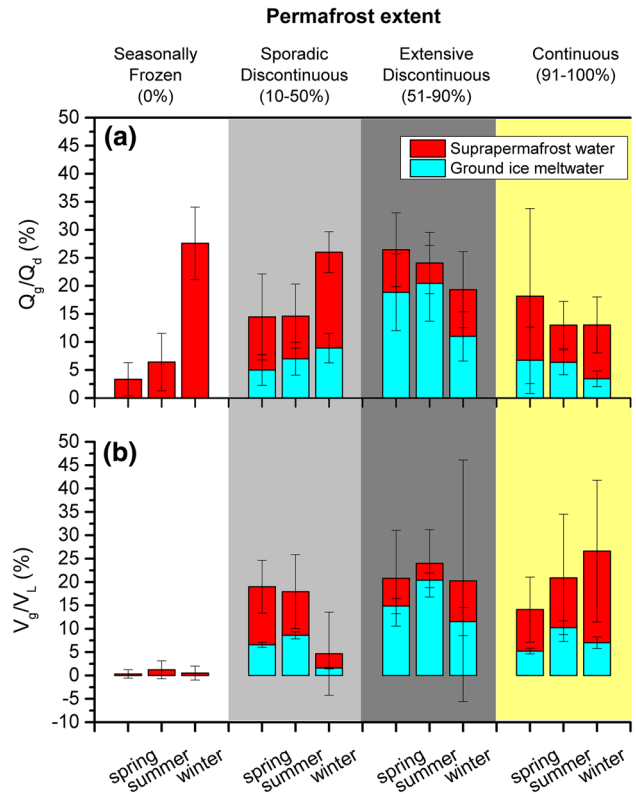


Fig. 6 The estimated contribution ratios of groundwater and ground ice to tributary flow (**a**) and lake water volume (**b**) at zones with different permafrost extents in the three seasons. Error bars represent \pm standard error

(< 5%) in the groundwater proportions is persistently observed at both for extensive discontinuous permafrost and continuous permafrost areas from spring to summer and from summer to winter. The maximum contribution of thawing permafrost (ground ice) accounts for roughly 10–20% of tributary flow for extensive discontinuous permafrost, while in other permafrost regions it accounts for less than 10%.

The extremely low V_g/V_L ratio at seasonally frozen ground sites suggests little input of groundwater discharge to lakes. For extensive discontinuous permafrost and continuous permafrost areas, intra-annual changes of groundwater contributing to lake water remain relatively constant (< 7%) compared with the seasonal deviations noted for sporadic discontinuous permafrost, where the contributions of subsurface source are stable at around 20% in spring and summer but drop in the winter season to less than 5% of the lake volume. The spatial and temporal patterns of thawing permafrost released to lakes are in agreement with the results displayed in tributaries, the only exception being that almost no contribution of meltwater from ground ice to the lakes is found at sporadic permafrost sites in the winter season.

Discussion

Complexities and dissimilarities in the role of groundwater as well as thawing permafrost contributions to rivers and lakes is postulated to account not only for seasonal variations but also for patterns noted across trajectories of permafrost extent, as demonstrated by the isotopic evidence and IMB model results. Overall, our estimated proportions of groundwater contributions to river flow are summarized as follows: seasonally frozen ground (3–28%), discontinuous permafrost (13–28%), and continuous permafrost (13–19%). Similarly, lake water volume derived from groundwater is estimated as follows: seasonally frozen ground (0.3–1.2%), discontinuous permafrost (4.7–24.0%) and continuous permafrost (14.1–26.6%). While based on more extensive datasets, these values are highly consistent with previous observational snapshots in this study region, and concur with previous studies conducted outside the SAYR within similar seasonally frozen or permafrost-affected regions within the QTP. For example, groundwater discharge was found to account for 30% of the total river discharge in the Yellow River downstream of Zone 1 [20]. For a small sporadic discontinuous permafrost basin near Zone 2 only 20% of river discharge was generated from groundwater [19] which falls within the range of our findings. A hydrograph separation based on stable isotopes and hydro-chemical tracers indicated the contributing ratio of groundwater discharge to the river runoff varied seasonally from 10 to 50% in a catchment covered by extensive discontinuous permafrost area [15], which is similar to our findings for extensive discontinuous permafrost areas of Zone 3. The previously noted study also concluded that melting of ground ice was an important source of recharge to streamflow, reaching ratios of 24–32% in August [17], consistent with our findings for similar terrain. Ground ice meltwater contributions of 37% of total streamflow from a hydrograph separation study in Kunlun Mountains Pass in northern QTP [16] also echo similar results. Groundwater contributions ranging from –20 to 22% of the lake water storage in a permafrost degrading area in northeast of QTP [20] are consistent with our finding of minor groundwater input (6–13% of the total lake water volume) to a small lake in Zone 4 in the warm season.

In the discussion below, we first address the uncertainties and limitations in the IMB approach mainly resulting from the basic assumptions and measurement uncertainties associated with isotopes and physical parameters. Then, the hydrological effects of permafrost degradation on surface and subsurface water system are illustrated, which may provide the guidance of reducing biases when using IMB models and some referential consequences of hydrological and environmental changes by permafrost degradation.

Model validation and uncertainties

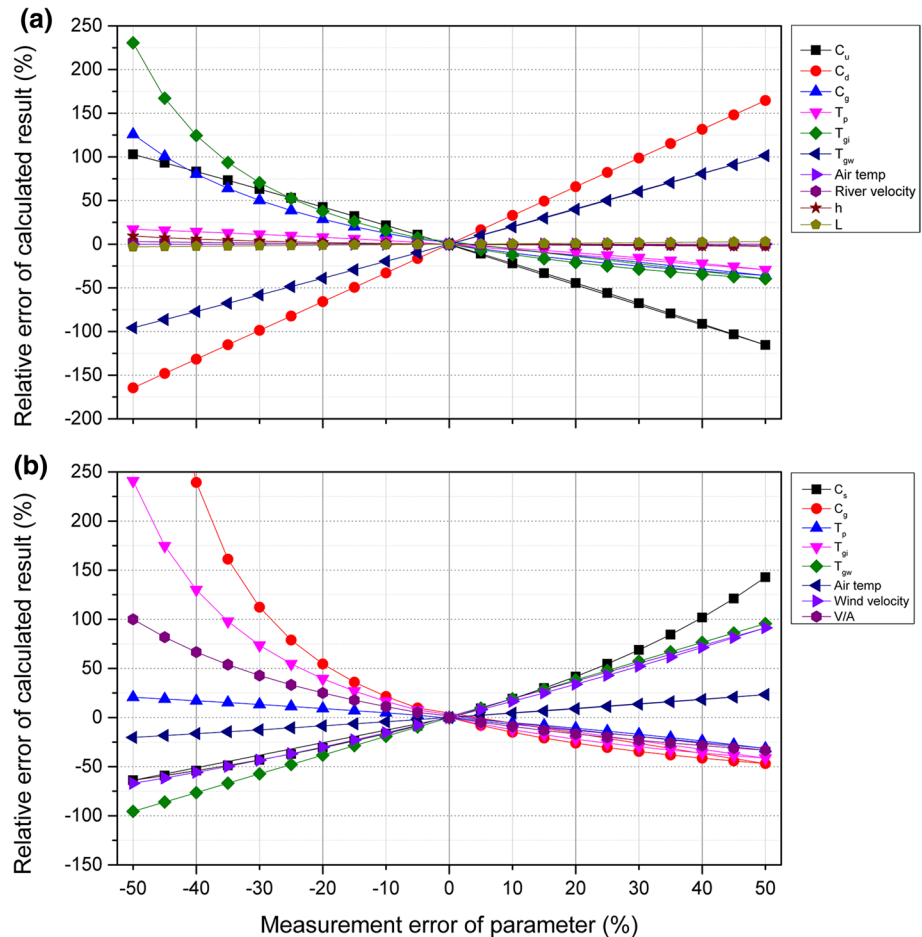
The basic assumptions of our revised approach are anchored in the fundamentals of water mass balance and isotope mass balance. The water mass balance is simplified to consider the subsurface flow to be the only source of recharge, which is assumed to account for any net increase in downstream discharge in Eq. (1). Hence, during our sampling period there were no precipitation events as shown in Fig. 2, which proves this assumption of water mass balance to be reasonable, and the considerable increment of ^{222}Rn activities in all downstream rivers including streams and tributaries also suggests the existence of progressive groundwater discharge. Previous studies have indicated that groundwater discharge will result in continuous increases in ^{222}Rn activities along a tributary reach, so the Eq. (2) is likely valid for the isotope mass balance [19]. The only possibly shortcoming of the model is that ^{222}Rn sources from production of ^{226}Ra decay are neglected, although the released ^{222}Rn from dissolved ^{226}Ra and sediments are often shown experimentally to be minor [20].

However, for quantification of thawing permafrost to groundwater and to rivers and lakes, we simply regard the groundwater in permafrost regions as well mixed combinations of precipitation and melted ground ice, which can be differentiated due to temporal changes in tritium since the 1950s bomb pulse, and display representative ranges largely reflecting origin and timing of formation (Figs. 3a, 4a). Use of average values of tritium concentrations in present-day precipitation underestimates the proportion of ground ice meltwater contributing to river flow and lake water volume, as tritium in present-day rainfall is relative low (< 10 T.U.; Fig. 3a) compared with historic tritium records in precipitation in this study area. If preserved in isolation until today, 1987–1988 precipitation would have a remaining tritium concentration of 14 T.U [18]. The groundwater is suggested to turnover a timescale of 1–4 years, it is possible that sub-permafrost water with average ages of up to 30 years to be incorporated in the groundwater discharge, as permafrost degradation is expected lead to deeper migration of flow-paths as well as increased flow rates [6]. Here the results still provide reasonable estimates of minimum contributions from thawing permafrost, and nevertheless, allow meaningful site-to-site intercomparisons [45, 46].

Even under ideal IMB conditions with valid assumptions, measurement errors in practical applications contribute to uncertainties in our estimations. As shown in Fig. 7a, b, a sensitivity analysis is used to illustrate potential errors associated with uncertainty in individual parameters used in the IMB [see also 27].

It is clear that the estimated proportion of ground ice meltwater contributing to river flow is potentially sensitive to all measurement deviations of radioactive isotope

Fig. 7 Relative errors in the calculated proportions of ground ice meltwater **a** to river discharge and **b** to lake water volume due to measurement errors of various parameters including radioactive isotope concentrations, meteorological data and hydrological characteristics



activities in all water bodies, while the calculated proportion of ground ice meltwater contributing to lake water volume seems to be sensitive to all parameters except air temperature. When the measurement error is at $\pm 5\%$ in the river model, the relative errors of targeted result caused by all parameters are less than 10%, the only exceptions are ^{222}Rn activities in upstream and downstream river water which result in 11% and 16% of the absolute values of relative error in targeted result respectively. However, when the measurement error reaches $\pm 20\%$, the absolute values of relative errors of targeted result caused by the measurement errors of isotope activities and other parameters vary significantly, from 8 to 66%, and from 0 to 1%, respectively. When it comes to lake models, a measurement error of $\pm 5\%$ placed on all parameters will produce of the absolute relative errors to be less than 10% in targeted result. When the measurement errors vary from 10 to 50%, the absolute values of relative errors increase sharply for all parameters except air temperature. The $\pm 20\%$ measurement error in isotope activities will bring in high relative error which can be up to 54%, and the $\pm 20\%$ measurement error in wind velocity will lead the relative error of targeted result to rise to 34% as well.

It should be noted that we use only standard errors caused by uncertainties in isotopic measurements in the model results. For other parameters such as flow velocity, wind velocity, climatic data, average depth of river and lake hydrological characteristics, measurement errors are difficult to evaluate. The analytical uncertainties in measurement of tritium concentrations are less than 5%, while measurement of ^{222}Rn activities varies between 2 and 22%. Thus, given that uncertainties in physical measurements are less than 10%, modelling results with uncertainties less than 20% are acceptable for the purpose of water resource management [27]. A high frequency of sampling and improvements in accuracy of parameter measurements will help reduce the uncertainties in future and ensure reliable results.

It should be acknowledged that isotopic signatures and modelling results derived in the sampling sites only represent a random snapshot of conditions over time, which is likely the most significant uncertainty in our study. Interannual variability of hydrological processes arising due to the unique setting of individual landscapes or climate conditions and drivers may inherently mask the site-to-site patterns [46]. The limitations of data availability are unavoidable, although our study is the first to provide

quantitative comparisons on the contribution of thawing permafrost to surface and subsurface runoff systems across a spatially diverse set of four permafrost and seasonally frozen soil landscapes in the QTP, a region vulnerable to climate change. In the following discussion we provide some important insight and synthesis of the hydrological drivers for various landscapes.

Hydrological implications of permafrost degradation

Since the 1980s, the general trend of permafrost degradation in the SAYR under warming conditions has been a transition from continuous permafrost regime to development of a progressively complex and irregular mosaic of contrasting discontinuous permafrost terrains, eventually progressing to sporadic permafrost, isolated patches of permafrost, and then to seasonally frozen ground once permafrost is completely thawed [28]. The modelling results presented here for tributaries and lakes within small catchments are valuable as quantitative indicators for comparison and differentiation of hydrological responses in the various permafrost-landscape units. Remarkable differences are noted in source contributions for the various terrains as noted below.

For continuous permafrost areas, thawing of permafrost accounts for less than half that of groundwater (Fig. 6a). In continuous permafrost systems, the permafrost table serves as an aquitard which restricts the vertical and in some cases, horizontal, movement of groundwater throughout a typical season. As a result, seasonal variations in groundwater contributions tend to be diminished compared to discontinuous permafrost areas [6]. Lower tritium concentrations in groundwater as compared to river water are typical, and combined with evidence of higher ^{222}Rn activities in rivers may suggest limited mobile subsurface storage (most being perennially frozen) as well as rapid response of precipitation and meltwater within the active layer being displaced to rivers [47]. Sub-permafrost groundwater is expected to be isolated from surface water due to streambeds and lakebeds being frozen and talik-free. Meanwhile, shallow thermokarst lakes may begin to form due to top-down thawing of permafrost, especially in the cold seasons when lakes may act as local heat storage reservoirs which eventually weaken soil refreezing and further accelerate the disappearance of permafrost in surrounding areas. Groundwater inputs to downstream water bodies may be enhanced as a result (Fig. 6b) [48].

In transitioning from continuous permafrost to extensive discontinuous permafrost, the proportion of thawing permafrost contributing to rivers and lakes increases two-fold as frozen ground becomes less thermally stable. Moreover, the increase in proportions of melting ground ice recharging to rivers and lakes appears also to induce increases in

proportions of groundwater discharge to rivers. These findings confirm that permafrost degradation directly promotes movement of permafrost meltwater to surface water bodies. A similar phenomenon is also reported in northeastern Alberta, Canada, where permafrost meltwater was inferred to be released to unfrozen wetlands and subsequently contributed to recharge in thermokarst lakes [24]. While extremely high tritium concentrations are detected both in lake water and groundwater in the SAYR during the warm season, rivers (other than rivers in extensive discontinuous permafrost) are not as seasonally responsive (Fig. 4a). Storage of permafrost meltwater in newly thawed subsurface aquifers appears to be an important process both in relation to regulation of thermokarst lake inputs and streamflow contributions, and may eclipse precipitation as indirect conveyors of meltwater to these water bodies [16, 17, 43, 46].

The landscape of the SAYR is expected to become dominated by sporadic and/or isolated discontinuous permafrost as permafrost degradation proceeds. Due to the substantial disappearance of impermeable permafrost, consequently, the prominent decrease in proportions of ground ice contributing to river discharges directly leads to the decline of meltwater and groundwater contributions to rivers, especially in the warm season (Fig. 6a). While the enlarged underground water storage capacity is also expanded due to deepening of active layer, the groundwater table generally will subside also. Potential mobilization of deep, tritium free groundwater as well as higher proportions of tritium depleted modern recharge is buffered by deeper groundwater levels and reduction in precipitation-induced runoff generation [13]. Logically, it follows that groundwater and meltwater induced runoff is weakened and delayed in warm seasons, but progressive release of water is expected to maintain baseflow in cold seasons, as further confirmed by the higher ^{222}Rn activities in winter (Fig. 4b) [12]. Also, hydraulic connections and subsurface flowpaths previously frozen would be influenced and reopened, and open taliks may cause the drainage of thermokarst lake water to subsurface aquifers. As a result, especially during the ice-covered period, groundwater recharge to lakes may be subdued [48, 49].

Ultimately in seasonally frozen ground, greater fluctuations in seasonal and intra-annual water balances may be realized once the buffering effect of meltwater is exhausted. Extreme drought-flood cycles including alteration in thaw lake distributions have also been suggested when permafrost is completely exhausted and may lead to increase in either low water levels or flood risk [3]. Regional water balances are likely to be significantly altered, which is likely to impact downstream flow conditions in the Yellow River and similar large rivers.

The linear regressions in Fig. 5b indicates contributions of groundwater discharge as well as thawing permafrost are the key components influencing water yield capacity

of catchment across the permafrost thaw gradient. While groundwater accounts for 88.3% of the total water resource in SAYR [6], from upstream to downstream (R1–R3), the average runoff depths are decreasing, which means most groundwater containing permafrost meltwater is not being supplied to streamflow but is retained in big lakes, thermokarst lakes and/or deeper groundwater aquifers, as permafrost degradation also modifies conditions controlling water drainage and connectivity [7]. The stability of local water resources is confirmed to be significantly influenced by climate changes and by the related degradation of permafrost currently underway and likely to continue in future across the SAYR.

Conclusions

Isotope mass models are developed by combining tritium concentrations and ^{222}Rn activities to quantify the contributions of groundwater and thawing permafrost to streamflow, tributary flow and lake water volume across four permafrost-related landscape types, in the Source Area of the Yellow River, northeastern part of the Qinghai-Tibet Plateau. The spatial and seasonal variations in the influences of groundwater and melting ground ice on rivers and lakes caused by landscape conditions and permafrost degradation have been revealed. Presence of extensive permafrost is found to restrict groundwater infiltration leading to responsive watershed hydrology. Sustained permafrost degradation in the region is expected to release large volumes of meltwater to rivers and is likely to enhance development and expansion of thermokarst lakes, however, enhanced subsurface water storage is expected to impact downstream water bodies by potentially delaying movement of surface and subsurface water. As a result, thawing permafrost may be less responsive to snow and rainfall events. At the later stage of permafrost degradation, large intra-annual variability in runoff discharge may occur.

The modelled results from this study are in broad agreement with some previous studies, even considering uncertainties and limitations in the methods applied. The combination of radon and tritium methods presented here is a new approach expected to be effective for hydrological and environmental characterization of spatial and temporal changes in remote, permafrost-affected regions where long-term hydrological monitoring is sparse or absent. Ongoing research is aimed to further testing the robustness of the methodology, and gaining further insight into the role of permafrost and permafrost degradation on the water cycle in critical regions.

Acknowledgements This research was fully supported by the Postgraduate Research & Practice Innovation Program of Jiangsu Province

(Grant No. KYCX17_0418) and the Fundamental Research Funds for the Central Universities (Grant No. 2017B682X14), and partially funded by the State Key Program of National Natural Science of China (Grant No. 51539003), the Strategic Priority Research Program of Chinese Academy of Sciences (XDA2010010307). The authors would like to express special thanks to Miss. Qian Chen for her enormous assistance with sample finishing.

References

1. Walvoord MA, Kurylyk BL (2016) Hydrologic impacts of thawing permafrost—a review. *Vadose Zone J.* <https://doi.org/10.2136/vzj2016.01.0010>
2. Li X, Cheng G, Jin H, Kang E, Che T, Jin R, Wu L, Nan Z, Wang J, Shen Y (2008) Cryospheric change in China. *Glob Planet Change* 62(3–4):210–218. <https://doi.org/10.1016/j.gloplacha.2008.02.001>
3. Ran Y, Li X, Cheng G (2017) Climate warming has led to the degradation of permafrost stability in the past half century over the Qinghai-Tibet Plateau. In: *The Cryosphere Discussions*, pp 1–30. <https://doi.org/10.5194/tc-2017-120>
4. Connon RF, Quinton WL, Craig JR, Hayashi M (2014) Changing hydrologic connectivity due to permafrost thaw in the lower Liard River valley, NWT, Canada. *Hydrol Process* 28(14):4163–4178. <https://doi.org/10.1002/hyp.10206>
5. Walvoord MA, Voss CI, Wellman TP (2012) Influence of permafrost distribution on groundwater flow in the context of climate-driven permafrost thaw: example from Yukon Flats Basin, Alaska, United States. *Water Resour Res* 48(7):1–17. <https://doi.org/10.1029/2011WR011595>
6. Cheng G, Jin H (2013) Permafrost and groundwater on the Qinghai-Tibet Plateau and in northeast China. *Hydrogeol J* 21(1):5–23. <https://doi.org/10.1007/s10040-012-0927-2>
7. Ala-Aho P, Soulsby C, Pokrovsky OS, Kirpotin SN, Karlsson J, Serikova S, Vorobyev SN, Manasypov RM, Loiko S, Tetzlaff D (2018) Using stable isotopes to assess surface water source dynamics and hydrological connectivity in a high-latitude wetland and permafrost influenced landscape. *J Hydrol* 556:279–293. <https://doi.org/10.1016/j.jhydrol.2017.11.024>
8. Brutsaert W, Hiyama T (2012) The determination of permafrost thawing trends from long-term streamflow measurements with an application in eastern Siberia. *J Geophys Res Atmos* 117(22):1–10. <https://doi.org/10.1029/2012JD018344>
9. St. Jacques JM, Sauchyn DJ (2009) Increasing winter baseflow and mean annual stream flow from possible permafrost thawing in the Northwest Territories, Canada. *Geophys Res Lett* 36(1):L01401. <https://doi.org/10.1029/2008gl035822>
10. Walvoord MA, Striegl RF (2007) Increased groundwater to stream discharge from permafrost thawing in the Yukon River Basin: potential impacts on lateral export of carbon and nitrogen. *Geophys Res Lett* 34(12):L12402. <https://doi.org/10.1029/2007GL030216>
11. Smith LC, Pavelsky TM, MacDonald GM, Shiklomanov AI, Lambers RB (2007) Rising minimum daily flows in northern Eurasian rivers: a growing influence of groundwater in the high-latitude hydrologic cycle. *J Geophys Res.* <https://doi.org/10.1029/2006JG000327>
12. Streletskiy DA, Tananaev NI, Opel T, Shiklomanov NI, Nyland KE, Streletskaya ID, Shiklomanov AI (2015) Permafrost hydrology in changing climatic conditions: seasonal variability of stable isotope composition in rivers in discontinuous permafrost. *Environ Res Lett* 10(9):95003. <https://doi.org/10.1088/1748-9326/10/9/095003>

13. Wu X, Zhang X, Xiang X, Zhang K, Jin H, Chen X, Wang C, Shao Q, Hua W (2018) Changing runoff generation in the source area of the Yellow River: mechanisms, seasonal patterns and trends. *Cold Reg Sci Technol* 155(June):58–68. <https://doi.org/10.1016/j.coldregions.2018.06.014>
14. Ge M, Wang S, Sun Z, Ma R, Hu Y, Chang Q, Xing W (2017) Hydrological connectivity from glaciers to rivers in the Qinghai-Tibet Plateau: roles of suprapermafrost and subpermafrost groundwater. *Hydrol Earth Syst Sci* 21(9):4803–4823. <https://doi.org/10.5194/hess-21-4803-2017>
15. Yang Y, Wu Q, Jin H (2016) Evolutions of water stable isotopes and the contributions of cryosphere to the alpine river on the Tibetan Plateau. *Environ Earth Sci* 75(1):1–11. <https://doi.org/10.1007/s12665-015-4894-5>
16. Yang Y, Wu Q, Yun H, Jin H, Zhang Z (2016) Evaluation of the hydrological contributions of permafrost to the thermokarst lakes on the Qinghai-Tibet Plateau using stable isotopes. *Glob Planet Change* 140:1–8. <https://doi.org/10.1016/j.gloplacha.2016.03.006>
17. Yang Y, Wu Q, Jin H, Wang Q, Huang Y, Luo D, Gao S, Jin X (2019) Delineating the hydrological processes and hydraulic connectivities under permafrost degradation on Northeastern Qinghai-Tibet Plateau, China. *J Hydrol* 569:359–372. <https://doi.org/10.1016/j.jhydrol.2018.11.068>
18. Yi P, Wan C, Jin H, Luo D, Yang Y, Wang Q, Yu Z, Aldahan A (2018) Hydrological insights from hydrogen and oxygen isotopes in Source Area of the Yellow River, east-northern part of Qinghai-Tibet Plateau. *J Radioanal Nucl Chem* 317(1):131–144. <https://doi.org/10.1007/s10967-018-5864-7>
19. Zheng MJ, Wan CW, Du MD, Zhou XD, Yi P, Aldahan A, Jin HJ, Luo DL, Yu ZB, Gong M (2016) Application of Rn-222 isotope for the interaction between surface water and groundwater in the Source Area of the Yellow River. *Hydrol Res* 47(6):1253–1262. <https://doi.org/10.2166/nh.2016.070>
20. Yi P, Luo H, Chen L, Yu Z, Jin H, Chen X, Wan C, Aldahan A, Zheng M, Hu Q (2018) Evaluation of groundwater discharge into surface water by using Radon-222 in the Source Area of the Yellow River, Qinghai-Tibet Plateau. *J Environ Radioact* 192:257–266. <https://doi.org/10.1016/j.jenvrad.2018.07.003>
21. Gao Z, Niu F, Lin Z, Luo J, Yin G, Wang Y (2018) Evaluation of thermokarst lake water balance in the Qinghai-Tibet Plateau via isotope tracers. *Sci Total Environ* 636:1–11. <https://doi.org/10.1016/j.scitotenv.2018.04.103>
22. Gibson JJ, Birks SJ, Yi Y (2016) Stable isotope mass balance of lakes: a contemporary perspective. *Quatern Sci Rev* 131:316–328. <https://doi.org/10.1016/j.quascirev.2015.04.013>
23. Petermann E, Gibson JJ, Knöller K, Pannier T, Weiß H, Schubert M (2018) Determination of groundwater discharge rates and water residence time of groundwater-fed lakes by stable isotopes of water (18O,2H) and radon (222Rn) mass balances. *Hydrol Process* 32(6):805–816. <https://doi.org/10.1002/hyp.11456>
24. Gibson JJ, Birks SJ, Yi Y (2016) Higher tritium concentrations measured in permafrost thaw lakes in northern Alberta. *Hydrol Process* 30(2):245–249. <https://doi.org/10.1002/hyp.10599>
25. Samalavičius V, Mokrik R (2016) Tritium activity trend formation in groundwater of Quaternary aquifer system, south-eastern Lithuania. *Geol Geogr*. <https://doi.org/10.6001/geol-geogr.v2i4.3399>
26. Bond MJ, Carr J (2018) Permafrost thaw and implications for the fate and transport of tritium in the Canadian north. *J Environ Radioact* 192(March):295–311. <https://doi.org/10.1016/j.jenvrad.2018.07.006>
27. Su X, Xu W, Yang F, Zhu P (2015) Using new mass balance methods to estimate gross surface water and groundwater exchange with naturally occurring tracer 222Rn in data poor regions: a case study in northwest China. *Hydrol Process* 29(6):979–990. <https://doi.org/10.1002/hyp.10208>
28. Jin H, He R, Cheng G, Wu Q, Wang S, Lü L, Chang X (2009) Changes in frozen ground in the source area of the yellow river on the qinghai-tibet plateau, China, and their eco-environmental impacts. *Environ Res Lett*. <https://doi.org/10.1088/1748-9326/4/4/045206>
29. Luo D, Jin H, Jin X, He R, Li X, Muskett RR, Marchenko RR, Romanovsky VE (2018) Elevation-dependent thermal regime and dynamics of frozen ground in the Bayan Har Mountains, north-eastern Qinghai-Tibet Plateau, southwest China. *Permafrost Periglac Process* 29(4):257–270. <https://doi.org/10.1002/ppp.1988>
30. Li J, Sheng Y, Wu J, Feng Z, Ning Z, Hu X, Zhang X (2016) Landform-related permafrost characteristics in the source area of the Yellow River, eastern Qinghai-Tibet Plateau. *Geomorphology* 269:104–111. <https://doi.org/10.1016/j.geomorph.2016.06.024>
31. Wang S, Sheng Y, Li J, Wu J, Cao W, Ma S (2018) An Estimation of Ground Ice Volumes in Permafrost Layers in Northeastern Qinghai-Tibet Plateau, China. *Chin Geogr Sci* 28(1):61–73. <https://doi.org/10.1007/s11769-018-0932-z>
32. Luo D, Jin H, Wu Q, Bense VF, He R, Ma Q, Gao S, Jin X, Lü L (2018) Thermal regime of warm-dry permafrost in relation to ground surface temperature in the Source Areas of the Yangtze and Yellow rivers on the Qinghai-Tibet Plateau, SW China. *Sci Total Environ* 618:1033–1045. <https://doi.org/10.1016/j.scitotenv.2017.09.083>
33. Wan C, Gibson JJ, Shen S, Yi Y, Yi P, Yu Z (2019) Using stable isotopes paired with tritium analysis to assess thermokarst lake water balances in the Source Area of the Yellow River, northeastern Qinghai-Tibet Plateau. *Sci Total Environ, China*. <https://doi.org/10.1016/j.scitotenv.2019.06.427>
34. Cook PG (2013) Estimating groundwater discharge to rivers from river chemistry surveys. *Hydrol Process* 27(25):3694–3707. <https://doi.org/10.1002/hyp.9493>
35. Ellins KK, Roman-Mas A, Lee R (1990) Using 222Rn to examine groundwater/surface discharge interaction in the Rio Grande de Manati, Puerto Rico. *J Hydrol* 115(1–4):319–341
36. Peng TH, Takahashi T, Broecker W (1974) Surface radon measurements in the north Pacific ocean station PAPA. *J Geophys Res* 79(12):1772–1780
37. Stellato L, Petrella E, Terrasi F, Belloni P, Belli M, Sansone U, Celico F (2008) Some limitations in using 222Rn to assess river-groundwater interactions: the case of Castel di Sangro alluvial plain (central Italy). *Hydrogeol J* 16(4):701–712. <https://doi.org/10.1007/s10040-007-0263-0>
38. Dimova NT, Burnett WC (2011) Evaluation of groundwater discharge into small lakes based on the temporal distribution of radon-222. *Limnol Oceanogr* 56(2):486–494
39. Dimova NT, Burnett WC, Chanton JP, Corbett JE (2013) Application of radon-222 to investigate groundwater discharge into small shallow lakes. *J Hydrol* 486:112–122
40. Gilfedder BS, Frei S, Hofmann H, Cartwright I (2015) Groundwater discharge to wetlands driven by storm and flood events: quantification using continuous Radon-222 and electrical conductivity measurements and dynamic mass-balance modelling. *Geochim Cosmochim Acta* 165:161–177. <https://doi.org/10.1016/j.gca.2015.05.037>
41. MacIntyre S, Fram J, Kushner P, O'Brien WJ, Hobbie J, Kling GR, Wanninkhof R, Chanton JP (1995) Trace gas exchange across the air-water interface in freshwater and coastal marine environments. In: *Biogenic trace gases: measuring emission from soil and water*. Blackwell, pp 52–97
42. Cartwright I, Morgenstern U (2018) Using tritium and other geochemical tracers to address the “old water paradox” in headwater catchments. *J Hydrol* 563:13–21. <https://doi.org/10.1016/j.jhydrol.2018.05.060>
43. Cartwright I, Morgenstern U (2016) Using tritium to document the mean transit time and sources of water contributing to a

- chain-of-ponds river system: implications for resource protection. *Appl Geochem* 75:9–19. <https://doi.org/10.1016/j.apgeochem.2016.10.007>
44. International Atomic Energy Agency (2016) Global network of isotopes in precipitation, WISER Database. http://www.naweb.iaea.org/napc/ih/IHS_resources_gnip.html. Accessed 30 Apr 2019
45. Gibson JJ, Birks SJ, Moncur M (2019) Mapping water yield distribution across the South Athabasca Oil Sands (SAOS) area: baseline surveys applying isotope mass balance of lakes. *J Hydrol Reg Stud* 21:1–13. <https://doi.org/10.1016/j.ejrh.2018.11.001>
46. MacDonald LA, Wolfe BB, Turner KW, Anderson L, Arp CD, Birks SJ, Bouchard F, Edwards TW, Farquharson N, Hall RI, McDonald I, White H (2016) A synthesis of thermokarst lake water balance in high-latitude regions of North America from isotope tracers. *Arct Sci* 3(2):118–149. <https://doi.org/10.1139/as-2016-0019>
47. Ala-Aho P, Soulsby C, Pokrovsky OS, Kirpotin SN, Karlsson J, Serikova S, Manasypov R, Lim A, Krickov I, Kolesnichenko LG, Laudon H, Tetzlaff D (2018) Permafrost and lakes control river isotope composition across a boreal Arctic transect in the Western Siberian lowlands. *Environ Res Lett* 13(3):034028. <https://doi.org/10.1088/1748-9326/aaa4fe>
48. Pan X, Yu Q, You Y, Chun KP, Shi X, Li Y (2017) Contribution of supra-permafrost discharge to thermokarst lake water balances on the northeastern Qinghai-Tibet Plateau. *J Hydrol* 555:621–630. <https://doi.org/10.1016/j.jhydrol.2017.10.046>
49. Smith LC (2005) Disappearing arctic lakes. *Science* 308(5727):1429. <https://doi.org/10.1126/science.1108142>

Publisher's Note Springer Nature remains neutral with regard to jurisdictional claims in published maps and institutional affiliations.